Send Orders for Reprints to reprints@benthamscience.net

Current Alzheimer Research, 2020, *17*, 000-000

RESEARCH ARTICLE

Hippocampal and Amygdalar Morphological Abnormalities in Alzheimer's Disease Based on Three Chinese MRI Datasets

Yuanyuan Wei[1,2], Nianwei Huang[1], Yong Liu[3,4,5,6], Xi Zhang[7*], Silun Wang[8*] and Xiaoying Tang[1*]

[1]Department of Electrical and Electronic Engineering, Southern University of Science and Technology, Shenzhen, Guangdong, China; [2]School of Biomedical Engineering, The University of British Columbia, Vancouver, BC, Canada; [3]Brainnetome Center, Institute of Automation, Chinese Academy of Sciences, Beijing, China; [4]National Laboratory of Pattern Recognition, Institute of Automation, Chinese Academy of Sciences, Beijing, China; [5]CAS Center for Excellence in Brain Science and Intelligence Technology, Institute of Automation, Chinese Academy of Sciences, Beijing, China; [6]School of Artificial Intelligence, University of Chinese Academy of Sciences, Beijing, China; [7]Department of Neurology, Nanlou Division, Chinese PLA General Hospital; National Clinical Research Center for Geriatric Diseases, Beijing, China; [8]YIWEI Medical Technology Co., Ltd, Shenzhen, Guangdong, China

Abstract: ***Background:*** Early detection of Alzheimer's disease (AD) and its early stage, the mild cognitive impairment (MCI), has important scientific, clinical and social significance. Magnetic resonance imaging (MRI) based statistical shape analysis provides an opportunity to detect regional structural abnormalities of brain structures caused by AD and MCI.

Objective: In this work, we aimed to employ a well-established statistical shape analysis pipeline, in the framework of large deformation diffeomorphic metric mapping, to identify and quantify the regional shape abnormalities of the bilateral hippocampus and amygdala at different prodromal stages of AD, using three Chinese MRI datasets collected from different domestic hospitals.

Methods: We analyzed the region-specific shape abnormalities at different stages of the neuropathology of AD by comparing the localized shape characteristics of the bilateral hippocampi and amygdalas between healthy controls and two disease groups (MCI and AD). In addition to group comparison analyses, we also investigated the association between the shape characteristics and the Mini Mental State Examination (MMSE) of each structure of interest in the disease group (MCI and AD combined) as well as the discriminative power of different morphometric biomarkers.

Results: We found the strongest disease pathology (regional atrophy) at the subiculum and CA1 subregions of the hippocampus and the basolateral, basomedial as well as centromedial subregions of the amygdala. Furthermore, the shape characteristics of the hippocampal and amygdalar subregions exhibiting the strongest AD related atrophy were found to have the most significant positive associations with the MMSE. Employing the shape deformation marker of the hippocampus or the amygdala for automated MCI or AD detection yielded a significant accuracy boost over the corresponding volume measurement.

Conclusion: Our results suggested that the amygdalar and hippocampal morphometrics, especially those of shape morphometrics, can be used as auxiliary indicators for monitoring the disease status of an AD patient.

ARTICLE HISTORY

Received: August 19, 2020
Revised: October 12, 2020
Accepted: December 22, 2020

DOI:
??????????????????????????????????

Keywords: Alzheimer's disease, mild cognitive impairment, shape analysis, MMSE, large deformation diffeomorphic metric mapping, multiple datasets.

1. INTRODUCTION

Alzheimer's disease (AD) is a neurodegenerative disease characterized by progressive cognitive and functional deficits as well as behavioral changes [1-3]. Clinically, progressive memory loss, cognitive impairment, and language disturbance are the main manifestations of AD, which seriously affect the lives of the elderly and bring a heavy burden to their families and the entire society. Currently, there are more than 35 million AD patients in the world, with the corresponding number being more than 9 million in China. By 2050, the global incidence of AD is expected to triple [4, 5]. At the same time, the annual burden of AD for an economic giant like China is estimated to exceed 1 trillion US dollars by 2050 [6]. Early detection and prevention have become important directions in the field of AD research and have important scientific, clinical and social significance.

*Address correspondence to these author at the Department of Neurology, Nanlou Division, Chinese PLA General Hospital; National Clinical Research Center for Geriatric Diseases, Beijing, China; Tel: (+86) 10-66937693; E-mail: zhangxi@301hospital.com.cn

*YIWEI Medical Technology Co., Ltd, Shenzhen, Guangdong, Block B, BGD. 10, Phase III, Tech-Eco Park, Nanshan, Shenzhen, Guangdong, China; Tel: (+86) 755-82332473; E-mail: lawrence.wang@szdrbrain.com

*Department of Electrical and Electronic Engineering, Southern University of Science and Technology, Shenzhen, Guangdong, China; Tel: (+86) 755-88015472; E-mail: tangxy@sustech.edu.cn

1567-2050/20 $65.00+.00 © 2020 Bentham Science Publishers

Currently, the severity and progression rate of AD is typically assessed by clinical examinations and neuropsychological tests, such as the Mini-Mental State Examination (MMSE) [7], mainly focusing on memory, attention, orientation, language, and learning. In the diagnosis of AD, the MMSE test is powerful, but its results could be subjective and easily affected by the patient's mental and physical state at the time of the test. It may also be late and relatively inefficient for patients to be diagnosed in this way, especially for patients at an early stage of AD, such as the mild cognitive impairment (MCI) [8]. Recently, magnetic resonance imaging (MRI) based analysis has been suggested to be capable of detecting AD at an early stage by quantifying the structural brain changes [9-11], which are very sensitive to the degeneration that occurs in MCI and AD [12] and has been extensively studied in the research of AD diagnosis criteria [13]. Early detection of AD based on structural brain changes will allow early intervention before significant functional damage or neuronal damage occurs.

In the past decade, volumetric analysis of the medial temporal lobe structures, especially the hippocampus and the amygdala, has drawn a lot of attention in AD-related structural MRI research [14]. Various studies have identified hippocampal and amygdalar volume atrophy in MCI and AD patients compared to the healthy control (HC) [15-18]. The main limitation of volumetric analysis is that it cannot provide detailed information about subregional changes and thus cannot accurately identify which part of the structure of interest is affected the most by the neuropathology of the disease. Recently, research focus has shifted to region-specific shape changes of the hippocampus and the amygdala as well as their relevance to AD manifestations. It has been shown that the regional shape characteristics of those two structures can improve imaging-based diagnostic accuracy of MCI and AD [19-21]. In addition, combining structural shape analysis and subregion segmentation of the hippocampus and the amygdala has been demonstrated to be useful in understanding how AD spreads within a single structure of interest and identifying which part of each of the two structures is mostly affected by the disease [20-27].

An earlier study on a relatively small group of subjects showed that the hippocampal atrophy induced by AD is region-specific rather than uniformly homogeneous [19]. A similar finding was also reported for the amygdala [22]. Novel shape analysis techniques that can track this type of local shape changes would be a promising research tool for the analysis and early diagnosis of AD. The large deformation diffeomorphic metric mapping (LDDMM) framework has been successfully employed in the statistical shape analyses of subcortical and ventricular structures using structural MRI from a large group of HC, MCI, and AD subjects [20, 21]. For MCI and AD, strong and significant local shape change patterns were found for both the hippocampus and the amygdala. The strongest hippocampal atrophy was detected at CA1 and the strongest amygdalar atrophy was detected at the basolateral complex [20]. Automated classification accuracy of MCI and AD using shape deformation features was significantly higher than that of using the structural volumes [20, 21]. These findings were then further confirmed in a study involving long-term follow-up subjects [23], by correlating shape change rates with cognitive deterioration rates [24, 26]. Follow-up studies using other types of MRI modalities [25] and structural network analysis [27] were also conducted. However, most previous studies centered on subjects from North America or Europe [19-24, 26, 27], or only investigated single-site subjects with a relatively small sample size [25]. A comprehensive multi-site study from other regions of the world is a strong need to compare and confirm the results from previous studies, which is the essential motivation of this study.

In this work, we employed a well-established shape analysis pipeline to assess the regional shape abnormalities of the bilateral hippocampus and amygdala in MCI and AD, using three Chinese MRI datasets collected from different domestic hospitals. The shape analysis pipeline has been used and validated in many previous studies to investigate region-specific structural abnormalities in various neurodegenerative diseases [20, 23-25, 28-36]. The main goal of this study is to identify and quantify the hippocampal and amygdalar shape abnormalities at different stages of the neuropathology of AD. In addition to studying the regional shape abnormalities, we also quantified the linkage between the structural shape patterns and cognitive decline as measured by MMSE. Findings have been analyzed at a subregion level by dividing each structure of interest into four parts: CA1, CA2, CA3 combined with dentate gyrus, and subiculum for the hippocampus; and basolateral, basomedial, centromedial, and lateral nucleus for the amygdala. The discriminative power of the hippocampal and amygdala shape characteristics has also been investigated.

2. MATERIALS AND METHODS

2.1. Dataset

In this study, we acquired our MRI datasets from three different Chinese hospitals (hospital A, hospital B, and hospital C), consisting of three groups of subjects: HC, MCI and AD. There were 281 subjects in total, of whom 74 were from hospital A, 88 were from hospital B, and 119 were from hospital C. Among them, 89 were HC, 80 were MCI, and 112 were AD. The inclusion and exclusion criteria followed a previous study [37] and are similar to the Alzheimer's Disease Neuroimaging Initiative (ADNI) dataset [38, 39]. There was no long-term follow-up information for our three datasets, and thus the MCI and AD subjects were not further divided into subgroups. Detailed clinical and demographic characteristics are presented in Table **1**. A general idea about each group's severity can be obtained through the MMSE score.

For subjects from hospital A, the MR images were acquired from a 3.0 T MR scanner (Magnetom Tril, Siemens, Germany). Sagittal T1-weighted MR images were acquired using a magnetization-prepared rapid gradient-echo (MPRAGE) sequence (TR/TE = 2000/2.6 ms, FA = 9°, matrix = 256 × 224, FOV = 256 mm × 224 mm, 176 continuous sagittal slices with 1 mm thickness). For subjects from hospital B, sagittal structural images with a resolution of 0.94 × 0.94 × 1.2 mm^3 were acquired using a 3D MPRAGE sequence with a 3.0 T GE MR system (GE Healthcare, Milwaukee, WI) using a standard head coil. The scanning parameters were as follows: TR = 2000 ms, TE = 2.6 ms, and FA = 9°. For subjects from hospital C, a 3.0 T Siemens MR

Table 1. Clinical and demographic information of the MRI dataset collected from three Chinese hospitals (A, B, and C).

Group	Hospital	No. of Subjects	Gender (Male/Female)	Age (mean±std)	MMSE (mean±std)	Intracranial Volume (mm^3)
HC	All	89	42/47	67.9438±7.1037	28.6292±1.2914	1215423±112545
	A	21	7/14	65.0476±8.1638	28.4762±1.3645	1166498±90583
	B	27	16/11	69.1852±6.4691	28.8889±1.0127	1188889±95564
	C	41	19/22	68.6098±6.6779	28.5366±1.4159	1257955±119337
MCI	All	80	38/42	71.3750±8.5245	25.6625±3.6351	1215569±118900
	A	18	10/8	70.1667±7.9354	21.9444±5.0465	1209421±136638
	B	28	15/13	74.4286±7.9229	26.8929±1.7917	1186340±129331
	C	34	13/21	69.5000±8.8223	26.6176±2.4743	1242895±95003
AD	All	112	46/66	69.4375±9.0978	15.7589±7.1323	1180563±117969
	A	35	17/18	65.7714±8.3034	10.1429±6.6913	1163864±117388
	B	33	9/24	72.6667±9.0646	19.6061±4.3871	1153427±111007
	C	44	20/24	69.9318±8.8775	17.3409±6.4805	1214199±117935

system (Skyra, Siemens, Germany) with a standard head coil was used to acquire the MR images. The structural scans were obtained using a 3D MPRAGE sequence with the following parameters: TR = 2530 ms, TE = 3.43 ms, FA = 90°, matrix = 256 × 256, FOV = 256 mm × 256 mm, slice thickness = 1 mm. Each volume comprised 192 sagittal slices with a resolution of 1 × 1 × 1 mm^3.

2.2. Data Processing

Volumetric segmentations of the bilateral amygdala and hippocampus were automatically obtained from the MRICloud platform (https://mricloud.org/). The MRICloud platform provides a fully-automated cloud service for brain segmentation using MPRAGE images based on a two-level Bayesian parameter estimation algorithm. More details of this segmentation algorithm can be found elsewhere [40, 41], in which the authors have demonstrated its superior performance, especially in segmenting the amygdala and the hippocampus. After that, the segmented binary volumes were converted into triangulated surfaces for subsequent statistical shape analysis in the framework of the LDDMM [20, 42].

Following that, for each structure of interest, we created a common template surface from the triangulated surfaces of all subjects across all three groups. All surfaces were first rigidly aligned to a common spatial position via rotation and translation. And then, the common template surface was estimated from all rigidly aligned surfaces using a Bayesian template estimation algorithm [43], the key of which is an approximation of the expectation-maximization algorithm [44].

After obtaining the template surface for each structure of interest, we computed a structure-specific diffeomorphic registration between the template and each target surface using the LDDMM-surface mapping algorithm [30, 45]. For a given target surface, the LDDMM-surface algorithm delivers a diffeomorphic transformation that can be applied to deform the template to be very close to the target. From each template-to-target LDDMM-surface mapping, a scalar field was calculated as the determinant of the Jacobian of the diffeomorphism from LDDMM-surface, measuring the degree of expansion or atrophy at each vertex on the template surface relative to each subject/target surface. We shall call this scalar field a deformation marker. For each structure, all subject-specific deformation markers are indexed in a common template space.

Both the amygdala and the hippocampus are composed of several subregions with unique functions. For a better analysis, we divided the amygdalar and hippocampal template surfaces into functionally meaningful subregions. This division was achieved by performing LDDMM-surface mapping between manually-delineated template surfaces of high-field (7T) segmentations and our "population-averaged" template surfaces to connect the two coordinate systems, and then transferring the boundary definitions of those high-field subregions to our template surfaces. More details of this subregion division methodology can be found in the study by Tang *et al*. [20]. The bilateral hippocampus was divided into four distinct subregions: CA1, CA2, CA3/dentate gyrus, and subiculum. The bilateral amygdala was also subsegmented into four distinct subregions: basolateral, basomedial, centromedial, and lateral nucleus.

2.3. Group Comparison Analysis

In our vertex-based statistical shape analysis, we quantified the degree of each structure's shape abnormality at each vertex of the template surface in each patient group (MCI or

AD) relative to the HC group. We employed the following statistical model

$$J_k(s) = \beta_{k,0} + \beta_{k,1}\gamma(s) + \sum_{cov} \alpha_{cov} X_{cov}(s) + \varepsilon_k(s),$$

where $J_k(s)$ is the deformation marker of subject s at vertex k of the template surface; $X_{cov}(s)$ are the covariates including gender, age, and the intracranial volume; $\gamma(s)$ is a binary group variable and equals to 0 if subject s belongs to the HC group and 1 otherwise; $\varepsilon_k(s)$ represents the random noise; $-\beta_{k,1}$ represents the degree of the group shape difference (atrophy or expansion) at vertex k. The parameters $\beta_{k,0}$, $\beta_{k,1}$, α_{cov} are estimated using the maximum likelihood estimation. We tested the null hypothesis that $\beta_{k,1} = 0$ simultaneously for all vertices. The statistical significance of a group difference is measured by a p-value obtained from Fisher's method of randomization, more details of which can be found elsewhere [20, 46]. Since the statistics were computed at all vertices of the triangulated template surface to correct for multiple comparisons, we adjusted the p-values to control the familywise error rate (FWER) at a level of 0.05 based on the maximum statistic method [47]. We also tested and quantified the volumetric group differences for all four structures. For the volume comparisons, we used the same linear regression model. But there was no need for multiple comparison correction since there was only one comparison for each single structure.

2.4. Classification Experiment

To quantify the discrimination capabilities of different morphometric biomarkers, a set of classification experiments were performed on both volumes and shape deformation markers of the hippocampus and the amygdala. Among the available machine learning algorithms, Support Vector Machine (SVM) is one of the most popular classification methods for constructing AD detection models [48-56]. As such, SVM was used to build our automated HC-vs-AD and HC-vs-MCI classifiers. Considering the running speed of software implementation, LIBSVM [57] was utilized to construct the SVM classifiers in our experiments. As the default setting in LIBSVM, the traditional C-support vector classification model [58] and the radial basis function (RBF) kernel [59] were chosen along with the regularization parameter $C = 1.0$ and the kernel parameter $\gamma = \frac{1}{\text{number of features}}$.

In each classification experiment, a stratified 10-fold cross-validation was applied, and this 10-fold cross-validation was repeated 10 times to get more stable results.

2.5. Correlating Morphometry with MMSE

We then examined whether the hippocampal and amygdalar morphometrics, in terms of both volume and shape, can predict the degree of cognitive impairment in AD as measured by MMSE. To do that, we quantified the association between the MMSE score and the volume as well as the shape deformation marker of each structure of interest using the Pearson correlation coefficient (PCC). We used age, sex, and the intracranial volume as the covariates when calculating the PCCs. p-values were used to measure the statistical significance of the correlations. In the shape-to-MMSE correlations, given that there are multiple correlation tests performed simultaneously at all vertices of each single structure's template surface, we need to correct for multiple correlations. The "maximum statistic" method was again used by controlling the FWER at a level of 0.05 [60]. In this study, we analyzed the volume-to-MMSE and shape-to-MMSE correlations in the disease group (a combination of MCI and AD).

3. RESULTS

3.1. Volume Analysis

The volumes, in terms of mean and standard deviations, of the hippocampus and the amygdala of each of the three groups (HC, MCI, and AD) are tabulated in Table **2**. Comparing the volumes of HC, MCI, and AD, we found volumetric reductions of the bilateral hippocampi and amygdalas in MCI and AD, and the volumes of the three groups followed the order of HC>MCI>AD. The corresponding p-values obtained from the volumetric group comparisons are shown in Table **3**. There was no significant group difference between HC and MCI in terms of the left amygdalar volume (p>0.05). The significant right amygdalar volumetric reduction was detected in the MCI group (p<0.05). The bilateral hippocampal volumes decreased significantly in MCI relative to HC (p<0.05). Comparing AD with HC, we found significant volumetric reductions of the bilateral hippocampi and amygdalas (p<2.50E-05) in AD. The classification results of the volumes of the hippocampus and the amygdala on HC-vs-AD and HC-vs-MCI tasks are tabulated in Table **4**. The bilateral amygdalas performed much better than the bilateral hippocampi in terms of HC-vs-AD classification, but there is no huge difference on the HC-vs-MCI classification task.

The volume-to-MMSE correlation results of the bilateral hippocampi and amygdalas, within the disease group (MCI and AD combined) are shown in Fig. (**1**). From the fitted lines and the PCC values, we found that MMSE correlated positively to the volume of each of the four structures of interest. The volume-to-MMSE correlations were stronger for the bilateral amygdalas than those for the bilateral hippocampi. Also, the volume-to-MMSE correlations were all statistically significant (p<0.05).

3.2. Shape Analysis

The p-values obtained from comparing the shapes of the four structures of interest between HC and MCI as well as HC and AD are also tabulated in Table **3**. As shown in that table, there was a significant shape difference between HC and MCI for the right amygdala (p<2.50E-05), but not for the left amygdala (p>0.05), being consistent with volume findings. For the bilateral hippocampi, significant shape differences between HC and MCI were detected (p<2.50E-05). Comparing AD and HC, we found significant AD-specific shape abnormalities of the bilateral amygdalas and hippocampi (p<2.50E-05). The corresponding classification results

Table 2. Mean and standard deviations of the volumes of the bilateral amygdalas and hippocampi of each of the three groups (HC, MCI, and AD) (in mm^3).

-	HC	MCI	AD
Left Amygdala	1623±156	1555±246	1289±265
Right Amygdala	1878±187	1724±334	1471±294
Left Hippocampus	3673±418	3442±461	3207±575
Right Hippocampus	3826±403	3545±499	3259±549

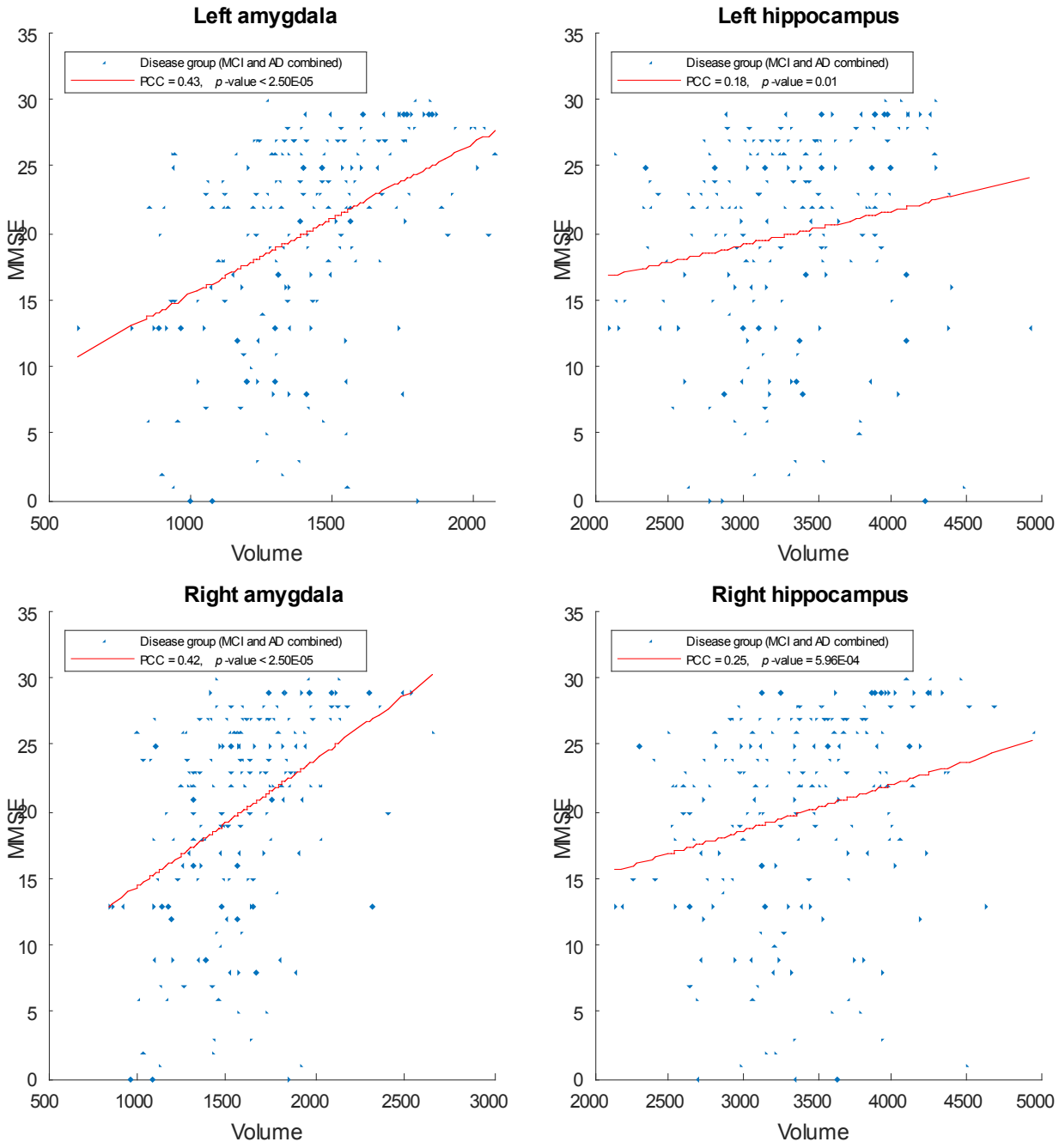


Fig. (1). The volume-to-MMSE correlation results of the bilateral amygdalas and hippocampi within the disease group (MCI and AD combined). (*A higher resolution / colour version of this figure is available in the electronic copy of the article*).

Table 3. A comparison of *p*-values obtained from the volume analysis and the shape analysis in comparing the bilateral amygdalas and hippocampi between HC and MCI as well as HC and AD.

-	HC vs. MCI		HC vs. AD	
-	Volume	Shape	Volume	Shape
Left Amygdala	0.12	0.06	<2.50E-05	<2.50E-05
Right Amygdala	1.00E-03	<2.50E-05	<2.50E-05	<2.50E-05
Left Hippocampus	1.00E-04	<2.50E-05	<2.50E-05	<2.50E-05
Right Hippocampus	1.00E-04	<2.50E-05	<2.50E-05	<2.50E-05

Table 4. The HC-vs-MCI and HC-vs-AD classification results by using volume and shape biomarkers of each of the four structures of interest.

-	HC vs. MCI		HC vs. AD	
-	Volume	Shape	Volume	Shape
Left Amygdala	57.34%±1.66%	62.31%±1.99%	82.49%±0.51%	84.78%±1.00%
Right Amygdala	64.97%±0.83%	66.39%±1.65%	80.65%±0.28%	83.78%±1.00%
Left Hippocampus	58.22%±1.58%	63.08%±1.58%	67.71%±0.64%	83.48%±0.56%
Right Hippocampus	66.27%±0.48%	69.41%±1.37%	73.63%±0.91%	83.78%±1.11%

of the shape characteristics of the four structures of interest, in terms of HC-vs-MCI and HC-vs-AD classifications, are tabulated in Table **4**. Compared to volume, the shape of each of the four structures of interest yielded much better classification results in terms of both HC-vs-MCI and HC-vs-AD.

The detailed region-specific shape findings of those four structures are demonstrated in Fig. (**2**) and Fig. (**3**). As shown in Fig. (**2**), no significant shape difference was detected between MCI and HC in the left amygdala. In the right amygdala, vertices belonging to almost every subregion exhibited localized surface atrophies in MCI relative to HC, with the degree of atrophy ranging from 6% to 13%. In AD, atrophies occurred at almost everywhere of the bilateral amygdalas, with the central region having the most severe atrophy (15%~20%).

As shown in Fig. (**3**), for the shape abnormalities of the bilateral hippocampi in MCI, we observed vertices belonging to the CA1, CA2 and subiculum subregions of the bilateral hippocampi exhibited localized surface atrophies in MCI relative to HC, with the degrees of atrophy ranging from 6% to 9%. The AD-related atrophies occurred at vertices belonging to almost every subregion, with the vertex-wise degrees of atrophy ranging between 13% and 25%. The most severe hippocampal atrophy occurred at vertices belonging mainly to the CA3 combined with Dentate Gyrus subregion and partially the CA1 and CA2 subregions.

Maps of the correlations between MMSE and the vertex-wise shape deformation markers of the bilateral hippocampi and amygdalas are demonstrated in Fig. (**4**). Statistically significant positive correlations were found between MMSE and the region-specific shape characteristics of the bilateral hippocampi and amygdalas. For the bilateral amygdalas, as shown in Fig. (**4**), significant regional shape-to-MMSE correlations were observed. Vertices belonging to each subregion had significant shape-to-MMSE correlations, with the strongest ones occurring mainly at the central region. This agrees well with the group comparison findings.

As shown in Fig. (**4**), significant positive correlations were also observed between the localized surface atrophies of the left hippocampus and MMSE, with the strongest correlation occurring at vertices belonging mainly to the CA1, CA2, and subiculum subregions. For the right hippocampus, significant shape-to-MMSE correlations were found at vertices belonging to almost every subregion.

4. DISCUSSION

In this paper, we employed a well-established statistical shape analysis pipeline to analyze the region-specific shape abnormalities of the bilateral hippocampi and amygdalas in MCI and AD. Specifically, we compared the localized shape characteristics of the bilateral hippocampi and amygdalas between HC and two disease groups (MCI and AD) using a relatively large MRI dataset obtained from three different Chinese hospitals. In addition to group comparison analyses, we also investigated the volume-to-MMSE and shape-to-MMSE associations of each structure of interest in the disease group (MCI and AD combined) as well as the MCI and AD discrimination abilities of different morphometric biomarkers.

Several findings have emerged from this study: (1) The volume of each of the four structures of interest had a tendency of HC>MCI>AD, which is consistent with existing

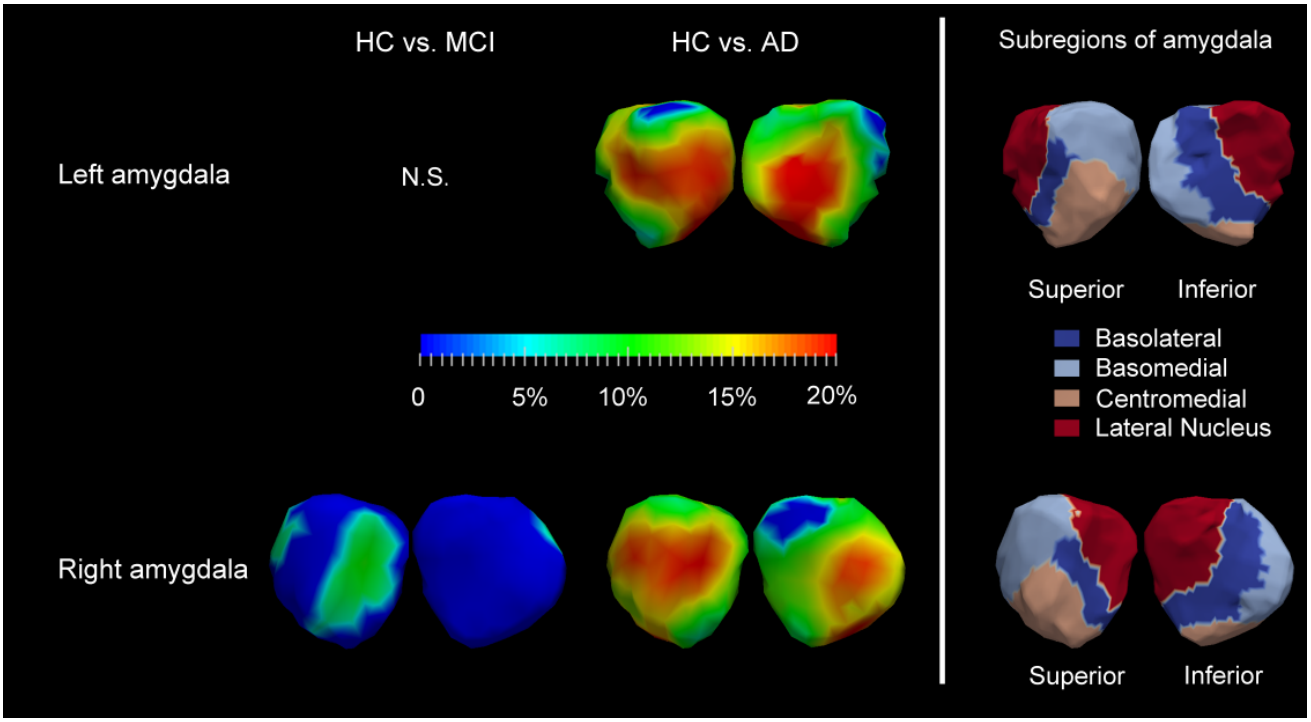


Fig. (2). Demonstration of the group shape differences of the bilateral amygdalas between HC and MCI, HC and AD, as well as the corresponding subregions. For figures in the left panel, the color bar denotes the percentage of atrophy in the disease group relative to that in HC. For figures in the right panel, the colordenotes each of the four amygdalar subregions. (*A higher resolution / colour version of this figure is available in the electronic copy of the article*).

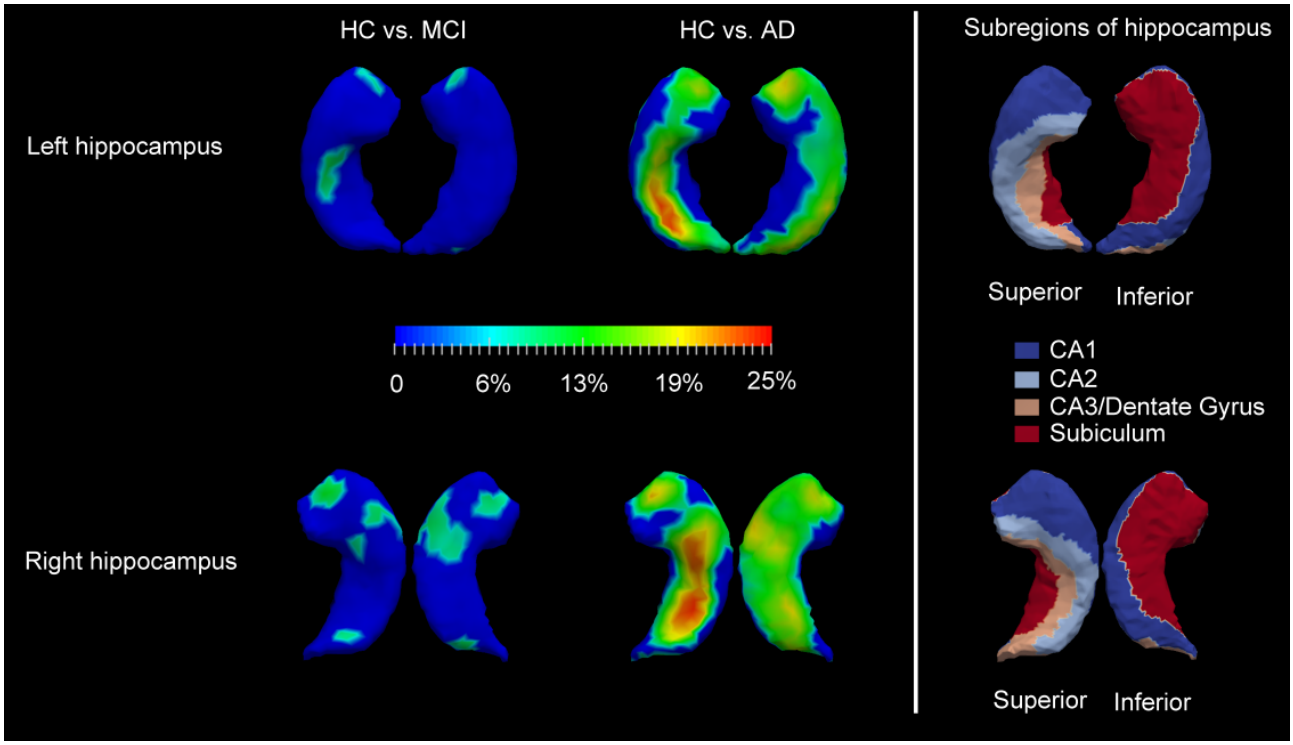


Fig. (3). Demonstration of the group shape differences of the bilateral hippocampi between HC and MCI,HC and AD, as well as the corresponding subregions. For figures in the left panel, the color bardenotes the percentage of atrophy in the disease group relative to that in HC. For figures in the right panel, the color denotes each of the four hippocampal subregions. (*A higher resolution / colour version of this figure is available in the electronic copy of the article*).

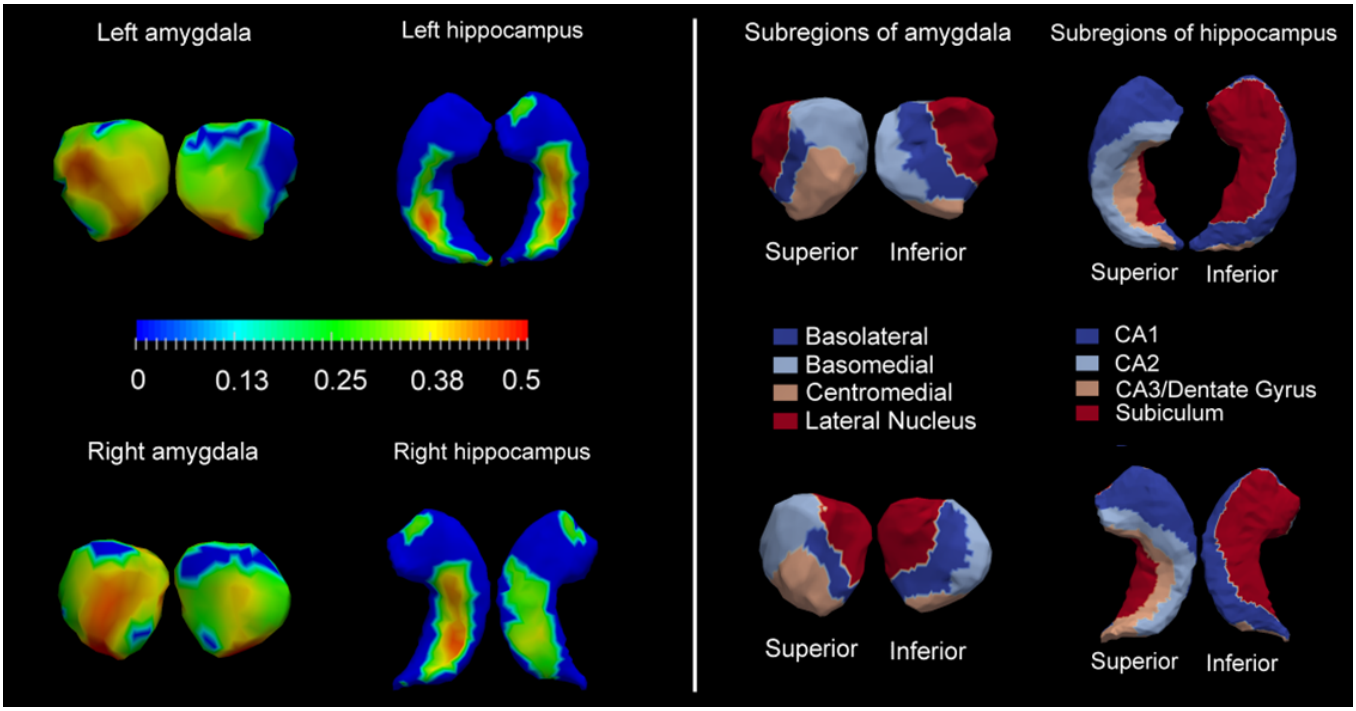


Fig. (4). Demonstration of the shape-to-MMSE correlations of the bilateral amygdalas and hippocampi within the disease group (MCI and AD combined), as well as the corresponding subregions. For figures in the left panel, the color bar denotes the PCC values. For figures in the right panel, the color denotes each of the four amygdalar and hippocampal subregions. (*A higher resolution / colour version of this figure is available in the electronic copy of the article*).

published results [18, 61, 62], suggesting that the volumes of those four structures may serve as auxiliary indicators for monitoring the disease status. (2) There were significant shape differences between MCI and HC for all four structures excluding the left amygdala. Significant region-specific AD-vs-HC shape differences were detected in all four structures, with a large number of surface vertices having been affected. (3) Overall, there existed vertices belonging to almost every subregion of each of the four structures of interest that had significant surface atrophies in AD relative to HC, with the most severe atrophy occurring at the CA3 combined with Dentate Gyrus subregion for the hippocampus and the central region (the basolateral and basomedial subregions) for the amygdala. (4) Significantly positive volume-to-MMSE and shape-to-MMSE correlations were observed for all four structures, and the shape regions showing the strongest correlations to MMSE agreed well with those exhibiting the strongest atrophies, both suggesting that the amygdalar and hippocampal morphometrics can be used as auxiliary indicators of the clinical status of an AD patient. (5) The shape biomarkers largely outperformed the corresponding volume biomarkers for each of the four structures of interest with respect to automated MCI and AD discriminations. This finding agrees well with our conjecture, given that shape provides more detailed morphological phenotype than volume and thus is more discriminating and sensitive to AD neuropathology. This would be the most important take-home message for clinicians, as now the practical guidance of incorporating shape biomarkers into the clinical AD diagnosis is still missing. One may anticipate that utilizing the complimentary information of shape and volume will provide new insights into the neuropathology of AD and further improve the early diagnosis accuracy of MCI and AD.

For bilateral hippocampi, the MCI-related abnormalities occurred at vertices belonging to the CA1 and subiculum subregions (see Fig. **3**). This roughly indicates that those two hippocampal subregions were affected the earliest in the neuropathology of AD, which is consistent with previous findings [20, 63-65]. In AD, region-specific atrophies occurred at almost every subregion of the hippocampus bilaterally. This agrees with the results from one of our previous works [20]. However, in this study, we found that the most severe hippocampal atrophy occurred at vertices mainly belonging to the CA3 combined with Dentate Gyrus subregion. This observation is somehow different from that of one of our previous works [20] focusing on AD patients from US and Europe but is consistent with another work, the subjects of which were recruited from China as well [25]. This may suggest that AD neuropathology is related to race, which needs to be further rigorously investigated in future research involving patients differing solely in race.

Despite its proximity to the hippocampus, relatively little is known about the role of the amygdala in AD. Recent shape analysis studies [20, 22, 23] have revealed substantial amygdalar atrophies in both MCI and AD. In our experiments, we found significant region-specific atrophies at every subregion of the bilateral amygdalas, with the strongest atrophy occurring at the central region, including the basolateral and the basomedial subregions. This is keeping in line with previous findings [20, 22]. For the amygdala, the abnormality patterns agree well with previous studies, of which

subjects were recruited from China as well as Europe and US.

CONCLUSION

In this study, because there was no long-term follow-up information for our three datasets, we could not analyze subgroup characteristics of MCI and AD nor correlate shape change rates with cognitive deterioration rates to confirm longitudinal findings from previous studies [21, 24, 26]. The APOE genotype was also unavailable despite its significant correlations to volume and shape morphometrics reported in a previous study [31]. These are the two major limitations of this study. In the future, analyzing subjects at different phases of the disease course (more refined than the MCI and AD categorizations) along with cognitive deterioration and genotype data will help better understand the disease pathology. In addition, future work will also focus on analyzing the shape morphometrics of other brain regions as well as combining more advanced machine learning techniques such as convolutional neural networks [66-70] and geometric deep learning [71-79] to design a much more accurate MCI and AD diagnosis system.

ETHICS APPROVAL AND CONSENT TO PARTICIPATE

Not applicable.

HUMAN AND ANIMAL RIGHTS

No Animals/Humans were used for studies that are base of this research.

CONSENT FOR PUBLICATION

Not applicable.

AVAILABILITY OF DATA AND MATERIALS

Not applicable.

FUNDING

None.

CONFLICT OF INTEREST

The authors declare no conflict of interest, financial or otherwise.

ACKNOWLEDGEMENTS

This study was supported by the National Key R&D Program of China (2017YFC 0112404, 2016YFC1305904) and the National Natural Science Foundation of China (NSFC 81501546, 81571062, 81471120).

REFERENCES

[1] McKhann G, Drachman D, Folstein M, Katzman R, Price D, Stadlan EM. Clinical diagnosis of Alzheimer's disease: Report of the NINCDS-ADRDA Work Group under the auspices of Department of Health and Human Services Task Force on Alzheimer's Disease. Neurology 34(7): 939 (1984).

[2] Woo H, Park J, Gwon A, Arumugam TV, Jo D. Alzheimer's disease and Notch signaling. Biochemical and Biophysical Research Communications 390(4): 1093-1097 (2009).

[3] Apostolova L. Alzheimer Disease. CONTINUUM: Lifelong Learning in Neurology 22(2): 419-434 (2016).

[4] Hebert L, Weuve J, Scherr P, Evans D. Alzheimer disease in the United States (2010–2050) estimated using the 2010 census. Neurology 80(19): 1778-1783 (2013).

[5] Weiner MW, Veitch DP, Aisen PS, Beckett LA, Cairns NJ, Cedarbaum J*, et al*. 2014 Update of the Alzheimer's Disease Neuroimaging Initiative: A review of papers published since its inception. Alzheimer's & Dementia: The Journal of the Alzheimer's Association 11(6): e1-e120 (2015).

[6] Keogh-Brown MR, Jensen HT, Arrighi HM, Smith RD. The Impact of Alzheimer's Disease on the Chinese Economy. EBioMedicine 4(C): 184-190 (2016).

[7] Folstein MF, Folstein SE, McHugh PR. "Mini-mental state": A practical method for grading the cognitive state of patients for the clinician. Journal of Psychiatric Research 12(3): 189-198 (1975).

[8] Petersen R. Mild Cognitive Impairment. CONTINUUM: Lifelong Learning in Neurology 22(2): 404-418 (2016).

[9] Wang J, Ekin A, de Haan G. Shape analysis of brain ventricles for improved classification of Alzheimer's patients. In: 2008 15th IEEE International Conference on Image Processing. IEEE. pp. 2252-2255 (2008).

[10] Arbabshirani MR, Plis S, Sui J, Calhoun VD. Single subject prediction of brain disorders in neuroimaging: Promises and pitfalls. NeuroImage 145: 137-165 (2017).

[11] Samper-González J, Burgos N, Bottani S, Fontanella S, Lu P, Marcoux A*, et al*. Reproducible evaluation of classification methods in Alzheimer's disease: Framework and application to MRI and PET data. NeuroImage 183: 504-521 (2018).

[12] Ramani A, Jensen JH, Helpern JA. Quantitative MR Imaging in Alzheimer Disease. Radiology 241(1): 26-44 (2006).

[13] Dubois B, Feldman HH, Jacova C, DeKosky ST, Barberger-Gateau P, Cummings J*, et al*. Research criteria for the diagnosis of Alzheimer's disease: revising the NINCDS–ADRDA criteria. The Lancet Neurology 6(8): 734-746 (2007).

[14] Yang S, Lee J, Huang C, Wang J, Hsu W, Wai Y. An Image-Aided Diagnosis System for Dementia Classification Based on Multiple Features and Self-Organizing Map. In: Neural Information Processing. Models and Applications. Berlin, Heidelberg: Springer Berlin Heidelberg. pp. 462-469 (2010).

[15] Karas GB, Scheltens P, Rombouts SARB, Visser PJ, van Schijndel RA, Fox NC*, et al*. Global and local gray matter loss in mild cognitive impairment and Alzheimer's disease. Neuroimage 23(2): 708-716 (2004).

[16] Basso M, Yang J, Warren L, MacAvoy MG, Varma P, Bronen RA*, et al*. Volumetry of amygdala and hippocampus and memory performance in Alzheimer's disease. Psychiatry Research: Neuroimaging 146(3): 251-261 (2006).

[17] Hořínek D, Varjassyová A, Hort J. Magnetic resonance analysis of amygdalar volume in Alzheimer's disease. Current Opinion in Psychiatry 20(3): 273-277 (2007).

[18] Poulin SP, Dautoff R, Morris JC, Barrett LF, Dickerson BC. Amygdala atrophy is prominent in early Alzheimer's disease and relates to symptom severity. Psychiatry Research: Neuroimaging 194(1): 7-13 (2011).

[19] Apostolova LG, Dinov ID, Dutton RA, Hayashi KM, Toga AW, Cummings JL*, et al*. 3D comparison of hippocampal atrophy in amnestic mild cognitive impairment and Alzheimer's disease. Brain : a journal of neurology 129(11): 2867-2873 (2006).

[20] Tang X, Holland D, Dale AM, Younes L, Miller MI. Shape abnormalities of subcortical and ventricular structures in mild cognitive impairment and Alzheimer's disease: Detecting, quantifying, and predicting. Human Brain Mapping 35(8): 3701-3725 (2014).

[21] Tang X, Holland D, Dale AM, Younes L, Miller MI. Baseline Shape Diffeomorphometry Patterns of Subcortical and Ventricular Structures in Predicting Conversion of Mild Cognitive Impairment to Alzheimer's Disease. Journal of Alzheimer's disease : JAD 44(2): 599-611 (2015).

[22] Cavedo E, Boccardi M, Ganzola R, Canu E, Beltramello A, Caltagirone C*, et al*. Local amygdala structural differences with 3T MRI in patients with Alzheimer disease. Neurology 76(8): 727-733 (2011).

[23] Miller MI, Younes L, Ratnanather JT, Brown T, Trinh H, Lee DS*, et al*. Amygdalar atrophy in symptomatic Alzheimer's disease based on diffeomorphometry: the BIOCARD cohort. Neurobiology of Aging 36: S3-S10 (2015).

[24] Tang X, Holland D, Dale AM, Younes L, Miller MI. The diffeomorphometry of regional shape change rates and its relevance to cognitive deterioration in mild cognitive impairment and Alzheimer's disease. Human Brain Mapping 36(6): 2093-2117 (2015).

[25] Tang X, Qin Y, Wu J, Zhang M, Zhu W, Miller MI. Shape and diffusion tensor imaging based integrative analysis of the hippocampus and the amygdala in Alzheimer's disease. Magnetic Resonance Imaging 34(8): 1087-1099 (2016).

[26] Gui L, Tang X, Moura JMF. Geodesic distance on a Grassmannian for monitoring the progression of Alzheimer's disease. NeuroImage 146: 1016-1024 (2017).

[27] Li J, Gong Y, Tang X. Hierarchical Subcortical Sub-Regional Shape Network Analysis in Alzheimer's Disease. Neuroscience 366: 70-83 (2017).

[28] Qiu A, Miller MI. Multi-structure network shape analysis via normal surface momentum maps. NeuroImage 42(4): 1430-1438 (2008).

[29] Miller MI, Younes L, Ratnanather JT, Brown T, Trinh H, Postell E*, et al*. The diffeomorphometry of temporal lobe structures in preclinical Alzheimer's disease. NeuroImage: Clinical 3: 352-360 (2013).

[30] Younes L, Ratnanather JT, Brown T, Aylward E, Nopoulos P, Johnson H*, et al*. Regionally selective atrophy of subcortical structures in prodromal HD as revealed by statistical shape analysis. Human Brain Mapping 35(3): 792-809 (2014).

[31] Tang X, Holland D, Dale AM, Miller MI. APOE Affects the Volume and Shape of the Amygdala and the Hippocampus in Mild Cognitive Impairment and Alzheimer's Disease: Age Matters. Journal of Alzheimer's disease : JAD 47(3): 645-660 (2015).

[32] Seymour KE, Tang X, Crocetti D, Mostofsky SH, Miller MI, Rosch KS. Anomalous subcortical morphology in boys, but not girls, with ADHD compared to typically developing controls and correlates with emotion dysregulation. Psychiatry Research: Neuroimaging 261: 20-28 (2017).

[33] Liu G, Tan X, Dang C, Tan S, Xing S, Huang N*, et al*. Regional Shape Abnormalities in Thalamus and Verbal Memory Impairment After Subcortical Infarction. Neurorehabilitation and Neural Repair 33(6): 476-485 (2019).

[34] Tang X, Ross CA, Johnson H, Paulsen JS, Younes L, Albin RL*, et al*. Regional subcortical shape analysis in premanifest Huntington's disease. Human Brain Mapping 40(5): 1419-1433 (2019).

[35] Tang X, Seymour KE, Crocetti D, Miller MI, Mostofsky SH, Rosch KS. Response control correlates of anomalous basal ganglia morphology in boys, but not girls, with attention-deficit/hyperactivity disorder. Behavioural Brain Research 367: 117-127 (2019).

[36] Zou L, Song Y, Zhou X, Chu J, Tang X. Regional morphometric abnormalities and clinical relevance in Wilson's disease. Movement Disorders 34(4): 545-554 (2019).

[37] Li A, Li J, Jin D, Liu Y, Liu B, Song C*, et al*. ASAF: altered spontaneous activity fingerprinting in Alzheimer's disease based on multisite fMRI. Science Bulletin 64(14): 998-1010 (2019).

[38] Mueller SG, Weiner MW, Thal LJ, Petersen RC, Jack CR, Jagust W*, et al*. Ways toward an early diagnosis in Alzheimer's disease: The Alzheimer's Disease Neuroimaging Initiative (ADNI). Alzheimer's & Dementia: The Journal of the Alzheimer's Association 1(1): 55-66 (2005).

[39] Jack CRJ, Bernstein MA, Fox NC, Thompson P, Alexander G, Harvey D*, et al*. The Alzheimer's Disease Neuroimaging Initiative (ADNI): MRI methods. Journal of Magnetic Resonance Imaging 27(4): 685-691 (2008).

[40] Tang X, Oishi K, Faria AV, Hillis AE, Albert MS, Mori S*, et al*. Bayesian Parameter Estimation and Segmentation in the Multi-Atlas Random Orbit Model. PloS one 8(6): e65591 (2013).

[41] Tang X, Crocetti D, Kutten K, Ceritoglu C, Albert MS, Mori S*, et al*. Segmentation of brain magnetic resonance images based on multi-atlas likelihood fusion: testing using data with a broad range of anatomical and photometric profiles. Frontiers in neuroscience 9: 61 (2015).

[42] Tang X, Luo Y, Chen Z, Huang N, Johnson HJ, Paulsen JS*, et al*. A Fully-Automated Subcortical and Ventricular Shape Generation Pipeline Preserving Smoothness and Anatomical Topology. Frontiers in neuroscience 12: 321 (2018).

[43] Ma J, Miller MI, Younes L. A Bayesian Generative Model for Surface Template Estimation. International journal of biomedical imaging 2010: 1-14 (2010).

[44] Dempster AP, Laird NM, Rubin DB. Maximum Likelihood from Incomplete Data via the EM Algorithm. Journal of the Royal Statistical Society. Series B (Methodological) 39(1): 1-38 (1977).

[45] Vaillant M, Glaunès J. Surface Matching via Currents. In: Information Processing in Medical Imaging. Berlin, Heidelberg: Springer Berlin Heidelberg. pp. 381-392 (2005).

[46] Younes L, Albert M, Miller MI. Inferring changepoint times of medial temporal lobe morphometric change in preclinical Alzheimer's disease. NeuroImage: Clinical 5(C): 178-187 (2014).

[47] Nichols T, Hayasaka S. Controlling the familywise error rate in functional neuroimaging: a comparative review. Statistical Methods in Medical Research 12(5): 419-446 (2003).

[48] Kloppel S, Stonnington CM, Chu C, ganski B, Scahill RI, Rohrer JD*, et al*. Automatic classification of MR scans in Alzheimer's disease. Brain 131(3): 681-689 (2008).

[49] Magnin B, Mesrob L, Kinkingnéhun S, Pélégrini-Issac M, Colliot O, Sarazin M*, et al*. Support vector machine-based classification of Alzheimer's disease from whole-brain anatomical MRI. Neuroradiology 51(2): 73-83 (2009).

[50] Zhang D, Wang Y, Zhou L, Yuan H, Shen D. Multimodal classification of Alzheimer's disease and mild cognitive impairment. NeuroImage 55(3): 856-867 (2011).

[51] O'Dwyer LG, Lamberton F, Bokde AL, Ewers M, Faluyi YO, Tanner C*, et al*. Using support vector machines with multiple indices of diffusion for automated classification of mild cognitive impairment. Plos One 7(2): e32441 (2012).

[52] Wee C, Yap P, Zhang D, Denny K, Browndyke JN, Potter GG*, et al*. Identification of MCI individuals using structural and functional connectivity networks. NeuroImage 59(3): 2045-2056 (2012).

[53] Wee C, Yap P, Shen D. Prediction of Alzheimer's disease and mild cognitive impairment using cortical morphological patterns. Human Brain Mapping 34(12): 3411-3425 (2013).

[54] Tang X, Qin Y, Zhu W, Miller MI. Surface-based vertexwise analysis of morphometry and microstructural integrity for white matter tracts in diffusion tensor imaging: With application to the corpus callosum in Alzheimer's disease. Human Brain Mapping 38(4): 1875-1893 (2017).

[55] Luo Y, Tang X. Automated diagnosis of Alzheimer's disease with multi-atlas based whole brain segmentations. In: Medical Imaging 2017: Biomedical Applications in Molecular, Structural, and Functional Imaging. SPIE. pp. 1013712 (2017).

[56] Wei Y, Chen Z, Tang X. Classifying Alzheimer's disease using probability distribution distance of fractional anisotropy and trace from diffusion tensor imaging in combination with whole-brain segmentations. In: Medical Imaging 2018: Biomedical Applications in Molecular, Structural, and Functional Imaging. SPIE. pp. 1057802 (2018).

[57] Chang C, Lin C. LIBSVM: A library for support vector machines. ACM Transactions on Intelligent Systems and Technology (TIST) 2(3): 1-27 (2011).

[58] Cortes C, Vapnik V. Support-vector networks. Machine Learning 20(3): 273-297 (1995).

[59] Scholkopf B, Sung K, Burges CJC, Girosi F, Niyogi P, Poggio T*, et al*. Comparing support vector machines with Gaussian kernels to radial basis function classifiers. IEEE Transactions on Signal Processing 45(11): 2758-2765 (1997).

[60] Groppe DM, Urbach TP, Kutas M. Mass univariate analysis of event-related brain potentials/fields I: A critical tutorial review. Psychophysiology 48(12): 1711-1725 (2011).

[61] Joko T, Washizuka S, Sasayama D, Inuzuka S, Ogihara T, Yasaki T*, et al*. Patterns of hippocampal atrophy differ among Alzheimer's disease, amnestic mild cognitive impairment, and late-life depression. Psychogeriatrics 16(6): 355-361 (2016).

[62] Dhikav V, Duraiswamy S, Anand KS. Correlation between hippocampal volumes and medial temporal lobe atrophy in patients with Alzheimer's disease. Annals of Indian Academy of Neurology 20(1): 29-35 (2017).

[63] Apostolova LG, Thompson PM, Green AE, Hwang KS, Zoumalan C, Jack CR*, et al*. 3D comparison of low, intermediate, and advanced hippocampal atrophy in MCI. Human Brain Mapping 31(5): 786-797 (2010).

[64] Lee P, Ryoo H, Park J, Jeong Y. Morphological and Microstructural Changes of the Hippocampus in Early MCI: A Study Utilizing the Alzheimer's Disease Neuroimaging Initiative Database. Journal of clinical neurology (Seoul, Korea) 13(2): 144-154 (2017).

[65] Su L, Hayes L, Soteriades S, Williams G, Brain SAE, Firbank MJ, *et al*. Hippocampal Stratum Radiatum, Lacunosum, and Moleculare Sparing in Mild Cognitive Impairment. Journal of Alzheimer's disease : JAD 61(1): 415-424 (2018).

[66] Krizhevsky A, Sutskever I, Hinton GE. ImageNet Classification with Deep Convolutional Neural Networks. In: Advances in Neural Information Processing Systems 25 (NIPS 2012). Curran Associates, Inc. pp. 1097-1105 (2012).

[67] Brosch T, Tam R. Manifold Learning of Brain MRIs by Deep Learning. In: Medical Image Computing and Computer-Assisted Intervention – MICCAI 2013. Berlin, Heidelberg: Springer Berlin Heidelberg. pp. 633-640 (2013).

[68] LeCun Y, Bengio Y, Hinton G. Deep learning. Nature 521(7553): 436-444 (2015).

[69] Suk H, Lee S, Shen D. Deep ensemble learning of sparse regression models for brain disease diagnosis. Medical Image Analysis 37: 101-113 (2017).

[70] Liu M, Zhang J, Adeli E, Shen D. Landmark-based deep multi-instance learning for brain disease diagnosis. Medical Image Analysis 43: 157-168 (2018).

[71] Scarselli F, Gori M, Tsoi AC, Hagenbuchner M, Monfardini G. The Graph Neural Network Model. TNN 20(1): 61-80 (2009).

[72] Masci J, Boscaini D, Bronstein MM, Vandergheynst P. Geodesic Convolutional Neural Networks on Riemannian Manifolds. In: 2015 IEEE International Conference on Computer Vision Workshop (ICCVW). IEEE. pp. 832-840 (2015).

[73] Bronstein MM, Bruna J, LeCun Y, Szlam A, Vandergheynst P. Geometric Deep Learning: Going beyond Euclidean data. IEEE Signal Processing Magazine 34(4): 18-42 (2017).

[74] Charles RQ, Su H, Kaichun M, Guibas LJ. PointNet: Deep Learning on Point Sets for 3D Classification and Segmentation. In: 2017 IEEE Conference on Computer Vision and Pattern Recognition (CVPR). IEEE. pp. 77-85 (2017).

[75] Monti F, Boscaini D, Masci J, Rodola E, Svoboda J, Bronstein MM. Geometric Deep Learning on Graphs and Manifolds Using Mixture Model CNNs. In: 2017 IEEE Conference on Computer Vision and Pattern Recognition (CVPR). IEEE. pp. 5425-5434 (2017).

[76] Fey M, Lenssen JE, Weichert F, Muller H. SplineCNN: Fast Geometric Deep Learning with Continuous B-Spline Kernels. In: 2018 IEEE/CVF Conference on Computer Vision and Pattern Recognition. IEEE. pp. 869-877 (2018).

[77] Gopinath K, Desrosiers C, Lombaert H. Graph Convolutions on Spectral Embeddings for Cortical Surface Parcellation. Medical Image Analysis 54: 297-305 (2019).

[78] Hanocka R, Hertz A, Fish N, Giryes R, Fleishman S, Cohen-Or D. MeshCNN. ACM Transactions on Graphics 38(4): 1-12 (2019).

[79] Zhao F, Xia S, Wu Z, Wang L, Chen Z, Lin W, *et al*. Spherical U-Net for Infant Cortical Surface Parcellation. In: 2019 IEEE 16th International Symposium on Biomedical Imaging (ISBI 2019). IEEE. pp. 1882-1886 (2019).